DOI 10.1007/s10717-023-00593-7
Glass and Ceramics, Vol. 80, Nos. 5 – 6, September, 2023 (Russian Original, Nos. 5 – 6, May – June, 2023)

UDC 666.3

FEATURES OF THE MICROSTRUCTURE AND THERMOELECTRIC PROPERTIES OF $Bi_2Te_{2.7}Se_{0.3}$ + Fe COMPOSITES WITH CORE–SHELL FILLER INCLUSIONS

A. E. Vasil'ev,[1, 2] O. N. Ivanov,[1, 3] M. N. Yapryntsev,[1, 2] and M. Zhezhu[2]

Translated from *Steklo i Keramika*, No. 6, pp. 60 – 68, June, 2023.

Original article submitted December 12, 2022.

Features of the thermoelectric properties and microstructure of composites with a matrix based on $Bi_2Te_{2.7}Se_{0.3}$ and an Fe filler were ascertained. A composition with filler weight content 0.3% Fe has a higher quality factor ZT compared to the $Bi_2Te_{2.7}Se_{0.3}$ matrix. For this composition the maximum value of ZT reaches about 0.75, while for $Bi_2Te_{2.7}Se_{0.3}$ ZT does not exceed about 0.63. So, in a composite of the system $Bi_2Te_{2.7}Se_{0.3}$ + Fe the thermoelectric quality factor can be increased by about 20%.

Keywords: ceramic-metal thermoelectric composites, core–shell inclusions, microstructure, thermoelectric properties.

INTRODUCTION

The cermet composites in the systems Bi_2Te_3 + M (M = Ni, Fe, Co) consist of a matrix based on the low-temperature thermoelectric material Bi_2Te_3 and a ferromagnetic filler. A distinctive microstructural feature of such composites is the formation in them of filler inclusions with a core–shell type internal structure [1 – 3]. The formation of Ni@$NiTe_2$, Fe@$FeTe_2$, and Co@$CoTe_2$ inclusions was confirmed for composites based on Bi_2Te_3 with Ni, Fe, and Co inclusions, respectively. The 'core' of the inclusions consists of ferromagnetic metal filler; the 'shell' corresponds to a new compound that is formed on spark plasma sintering of matrix and filler powder materials. The formation of a new compound is initiated by the diffusion redistribution of atoms of the matrix and filler materials at high temperatures. In turn, this redistribution leads to the corresponding solid-phase reaction of the type $Me^0 + 2Te^{2-} \rightarrow MeTe_2$ (Me = Ni, Fe, Co). An obvious approach to establishing the features of the thermoelectric properties of cermet composites with core–shell inclusions related to their microstructural features is based on investigating the effect of the filler content both on the thermoelectric properties themselves and on the microstructure.

The present article advances for the first time the results of an investigation of the features of the thermoelectric properties and microstructure of composites with a matrix based on $Bi_2Te_{2.7}Se_{0.3}$ and an Fe filler. The solid solutions $Bi_2Te_{3-x}Se_x$, which are semiconductors with electronic-type conductivity, are widely used in the creation of various low-temperature thermoelectric devices [4]. Iron is a ferromagnet with Curie temperature T_C = 1043 K.

OBTAINING SAMPLES; INVESTIGATION PROCEDURES

Spark plasma sintering was used to obtain bulk samples of the composite $Bi_2Te_{2.7}Se_{0.3}$ + xFe composite with different mass content of the filler (x = 0.0; 0.1; 0.3; 0.4, and 0.5%). For sintering, the initial $Bi_2Te_{2.7}Se_{0.3}$ and Fe powders were taken in the ratio corresponding to a certain value of x. Before sintering, the initial powders were thoroughly mechanically mixed for 2 h. Sintering was conducted at the following parameter values: pressure 40 MPa, temperature 723 K, sintering time 5 min, and atmospheric vacuum. An SPS 25/10 spark plasma sintering furnace was used. Commercial Fe powder (purity 99.995%, manufactured by OOO Khimkraft, Kaliningrad, Russia) was the filler. The Fe powder was

[1] National Research Technological University MISiS, Moscow, Russia (e-mail: alex19941005@mail.ru).
[2] Belgorod State National Research University, Belgorod, Russia (e-mail: yaprintsev@bsu.edu.ru).
[3] V. G. Shukhov Belgorod State Technological University, Belgorod, Russia (e-mail: olniv@mail.ru).

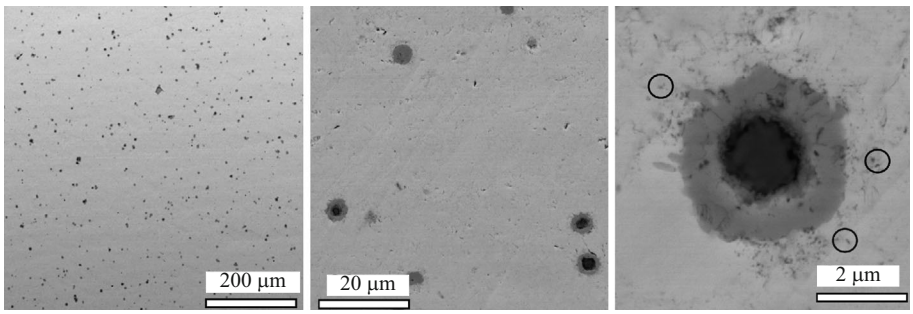

Fig. 1. BSE-SEM images of a polished surface of a composite sample with 0.5 wt.% Fe and with different magnifications (in the image on the right, the circles highlight individual nanometer inclusions of $FeTe_2$).

single-phase with a cubic structure (spatial symmetry group *Im*3*m* and unit cell parameters $a = b = c = 0.2867$ nm) and consisted of individual spherical agglomerated formations. The median diameter of the formations was about 3 μm. To obtain the initial $Bi_2Te_{2.7}Se_{0.3}$ powder, a polycrystal of the corresponding composition was first obtained by direct fusion of Bi, Te, and Se in a vacuum in a quartz ampul. The resulting polycrystal was ground for 8 h in a hexane medium in a planetary mill. The crushed powder consisted of particles of average size about 0.5 μm. The $Bi_2Te_{2.7}Se_{0.3}$ powder was also single-phase and corresponded to the rhombohedral symmetry group ($R\bar{3}m$) with parameters $c = 3.355$ nm and $a = b = 0.4354$ nm. The microstructural features of $Bi_2Te_{2.7}Se_{0.3} + x$Fe composite samples with different x were investigated by means of scanning electron microscopy (SEM, Quanta 600F scanning electron microscope), including SEM images obtained by means of the detection of backscattered electrons with different intensities (BSE-SEM method), SEM imaging method using backscattered electron diffraction (EBSD-SEM method), including a method of obtaining 'diffraction quality' maps (EBSD-IQ method), and energy dispersive x-ray spectroscopy (EDS, allows evaluation of elemental concentrations to within 0.1%).

Using a ZEM-3 setup, the electrical resistivity ρ of the samples was measured by the four-probe method to within 1% and the Seebeck coefficient S by the differential method to within 3%. Measurements of ρ and S were performed on bar-shaped samples with dimensions 2 × 2 × 10 mm. The full thermal conductivity k was measured on disk samples with dimensions ∅10 × 2 mm using a TC-1200H setup with a laser flash method to 5% accuracy.

EXPERIMENTAL RESULTS

The formation of both the required matrix–filler microstructure and the internal structure of the core–shell inclusions in the $Bi_2Te_{2.7}Se_{0.3} + x$Fe composite samples is confirmed by analyzing images of the polished surface of the composites obtained in the BSE-SEM regime. Such images, obtained with different magnifications, for a composite sample with 0.5 wt.% Fe are displayed in Fig. 1. Obviously, as a result of spark plasma sintering of $Bi_2Te_{2.7}Se_{0.3}$ and Fe powders, a characteristic microstructure of a composite that corresponds to the phases of a matrix and filler actually forms in the composite. In the BSE-SEM image obtained at minimum magnification (image on the left), the dark gray islands correspond to inclusions that are randomly distributed in a light gray matrix. The photo in the center shows several filler inclusions. It can be seen that the inclusions are of the core–shell type, i.e., have their own internal structure. A separate inclusion is displayed in the image on the right.

An earlier analysis of the elemental and phase compositions of the core and shell showed that the shell corresponds to the compound $FeTe_2$, and the core to Fe [3]. It was ascertained that texturing develops in all samples of the composite $Bi_2Te_{2.7}Se_{0.3} + x$Fe with different filler content. The development of texturing is confirmed by analyzing SEM images of surfaces that are perpendicular or parallel to the direction of pressing on spark-plasma sintering (Fig. 2). Texturing is conditioned by the ordering of lamellar grains of the polycrystalline material predominantly in a plane that is perpendicular to the direction of the applied pressure (this direction will be the axis of the texture). Texturing is a phenomenon typical of compounds based on Bi_2Te_3, which are obtained by means of technological methods, including uniaxial pressing by initial powders [5 – 8]. As shown in Fig. 2 the grains in the samples of the composite $Bi_2Te_{2.7}Se_{0.3} + x$Fe form the so-called lamellar structure, and the lamellar layers themselves are arranged perpendicular to the axis of texture. The platy grains stretch along the lamellar layers, as depicted in the SEM images of a 'parallel' surface. For a perpendicular surface, the grains are randomly oriented.

The principle stages of the formation of inclusions of the filler $Fe@FeTe_2$ in the composite $Bi_2Te_{2.7}Se_{0.3} + x$Fe are: first (starting) stage — hetero-diffusion redistribution of the atoms of the matrix materials on high-temperature sintering; second (principle) — solid-phase synthesis reaction of a new chemical compound in accordance with the formula $Fe^0 + 2Te^{2-} \rightarrow FeTe_2$.

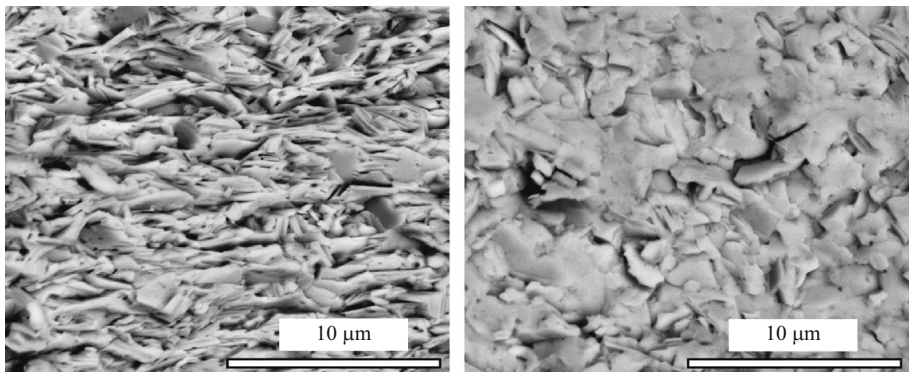

Fig. 2. SEM images of composite surfaces with 0.5 wt.% Fe, arranged perpendicular (on the left — 'perpendicular' surface) and parallel (on the right — 'parallel' surface) to the direction of pressing on sintering.

EDS spectra were obtained in different zones of the inclusion Fe@$FeTe_2$ (in the core, in a shell near the core, in a shell near the matrix material, and in matrix material far from an inclusion). The results of an elemental analysis of these zones are presented in Table 1. One can see that the inclusion core contains mainly Fe, the composite matrix consists mainly of Bi, Te, and Se, and the 'shell' contains both Fe atoms (filler element) and Bi, Te, and Se atoms (matrix material elements). Away from the core, the concentration of Fe decreases while the concentrations of Bi, Te, and Se, on the contrary, increase. Of note, the visualization of $FeTe_2$ inclusions using the IBSD-IQ method allows one to distinguish the shell as well as to obtain information about its microstructural features. On using this method the formation of diffraction contrast depends on the degree of imperfection of different surface elements of the sample under study.

Figure 3 shows an EBSD-IQ map of a composite sample with 0.5 wt.% Fe, obtained from a 'perpendicular' surface.

It is clear that a shell consists of many randomly oriented grains of irregular shapes and sizes equal to several hundred nanometers. Analysis of EBSD-SEM maps obtained from the surface of composite samples with different filler contents and oriented perpendicular to the axis of pressure application on sintering made it possible to determine the average grain size D and degree of texturing TF of the samples. As an example, such a map for a composite sample with 0.5 wt.% Fe is shown in Fig. 4. Each grain on such a map is colored according to the color coding associated in turn with the orientation of the crystallographic axes $\langle 0001\rangle$, $\langle 0\bar{1}10\rangle$, $\langle 1\bar{2}10\rangle$, and $\langle 1\bar{1}00\rangle$. The dependences $D(x)$ and $TF(x)$ for the $Bi_2Te_{2.7}Se_{0.3}$ + xFe composite are shown in Fig. 5. With an increase in the mass content of the filler, the average grain size gradually decreases from about 3 μm (x = 0% Fe) to about 0.8 μm (x = 0.5% Fe). The degree of texturing behaves in a more complex way: TF is maximum (about 6%) for a sample without filler, for a sample with a minimum filler content, TF is minimal (about 2.7%), and with a further increase in the filler content, and TF steadily increases.

Despite the noted features of the dependence $TF(x)$, the degree of texturing of all samples is quite low (for a completely textured sample with ideal grain ordering in any plane, TF = 100%, and for a completely non-textured sample with random grain orientation, TF = 0%.

To explain the features found in the behavior of the functions $D(x)$ and $TF(x)$ let the initial spherical agglomerated Fe formations with average size about 3 μm decompose into nanometer-sized particles as a result of mechanical mixing of the starting $Bi_2Te_{2.7}Se_{0.3}$ and Fe powders. Such particles are shown in the right-hand image of the inclusion in Fig. 1. Previously, such an effect was found for the composite

TABLE 1. Elemental Analysis of $FeTe_2$ Inclusion

Element	Content of elements, at.%			
	Core	Shell/core	Shell/matrix	Matrix
Fe	89.12	44.5	28.8	2.8
Se	1.06	1.4	7.3	14.0
Te	7.64	46.7	60.2	50.0
Bi	2.19	3.3	3.7	33.2

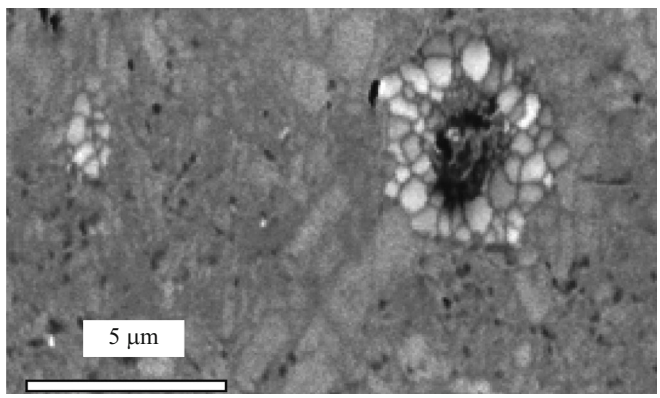

Fig. 3. EBSD-IQ-map of a composite sample with 0.5 wt.% Fe, obtained from a 'perpendicular' surface.

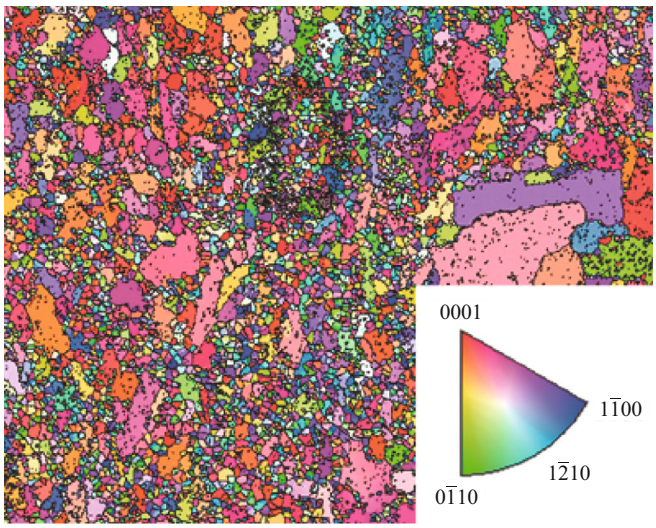

Fig. 4. EBSD-SEM map for a composite sample with 0.5 wt.% Fe obtained from a 'perpendicular' surface.

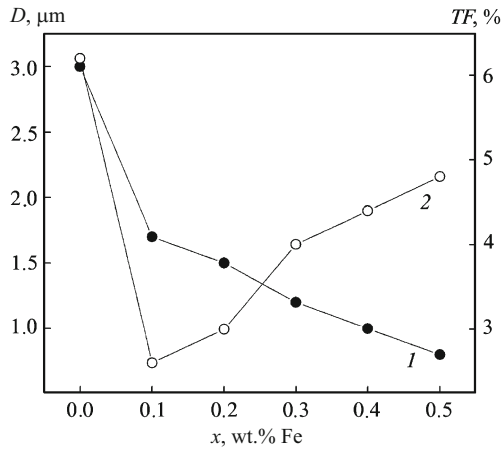

Fig. 5. Effect of the filler content on the average grain size (curve *1*) and the degree of texturing (curve *2*) of samples of the composite $Bi_2Te_{2.7}Se_{0.3}$ + *x*Fe composite.

Bi_2Te_3 + *x*Ni [1]. Then a reduction of the average grain size in samples of the composite $Bi_2Te_{2.7}Se_{0.3}$ + *x*Fe with increasing *x* can be caused by the fact that Fe nano-particles act as inhibitors of grain growth. The introduction of such growth inhibitors is a common method for controlling the grain structure in polycrystalline ceramic and metal materials [9, 10].

The same Fe nano- particles can significantly affect the development of texturing in the composites $Bi_2Te_{2.7}Se_{0.3}$ + *x*Fe. The initial stage of spark plasma sintering is the 'packing' of particles of the initial powder under the influence of external pressure on pressing [11]. On sintering of the composite $Bi_2Te_{2.7}Se_{0.3}$ + *x*Fe, particle packing will be accompanied by the alignment of randomly oriented particles in the initial $Bi_2Te_{2.7}Se_{0.3}$ powder into layers arranged perpendicular to the pressing direction. This preferential orientation of the powder particles will contribute to the further development of the texture in the bulk material sintered from the starting powder.

At the packing stage individual Fe nano-particles can act as a metallic lubricant. It is known that powders of some substances consisting of nano-particles actually exhibit such a lubricating effect, which effects more efficient packing of the particles of the initial powders on compaction. For example, the lubrication effect was found for Ce in the case of compaction of Al_2O_3 powder [12], and also for Te in the case of compaction of Bi_2Te_3 powder [13]. Then, a steady increase in *TF* with increasing filler content is simply a result of an increase in the content of metallic lubricant. Of note, however, this cannot be the only mechanism, since the maximum degree of texturing is observed for a composite sample without a filler. In this case, it is also necessary to take into account the possible effect of grain size on the degree of texturing.

Increase in texturing with decreasing grain size was previously observed in textured samples of $Bi_{2-x}Sm_xTe_{2.7}Se_{0.3}$ [1]. To explain this behavior the authors took into consideration the fact that the process of particle packing under uniaxial pressure includes two stages: particle rotation and particle sliding on particle contact. The sliding stage depends on the size of the particles in contact: an increase in particle size in the starting powder (resulting in a corresponding increase in grain size in the ceramic material sintered from powder) effects a high degree of ordering of the grains. This mechanism is described in detail in [1].

It was ascertained that all thermoelectric properties of samples of the composite $Bi_2Te_{2.7}Se_{0.3}$ + *x*Fe depend substantially on the filler content. In addition, the development of texturing in the samples resulted in thermoelectric anisotropy: the properties depended significantly on the direction of measurement. For this reason, the thermoelectric properties were measured in directions perpendicular (perpendicular to the orientation of measurement) and parallel (parallel to orientation measurement) to the axis of texture. The noted anisotropy of the transport properties is primarily a result of redistribution of contributions from the $a - b$ crystal plane (contributions ρ_{ab} and k_{ab}) and the crystal axis c (contributions ρ_c and k_c) to the electrical resistivity ρ and total thermal conductivity k of the textured samples.

For the parallel orientation of the measurement, the main contributions are ρ_c and k_c, and for the perpendicular orientation — ρ_{ab} and k_{ab} [4]. For compounds based on Bi_2Te_3, the anisotropy of transport properties is defined as $\rho_{ab} < \rho_c$ and $k_{ab} > k_c$. This means that the electrical resistivity will increase and the thermal conductivity will decrease for a parallel measurement orientation compared to a perpendicular measurement orientation. Since the thermoelectric properties for the perpendicular measurement orientation are better than the properties for the parallel measurement orientation, it is the properties measured for the perpendicular orientation that will be discussed below.

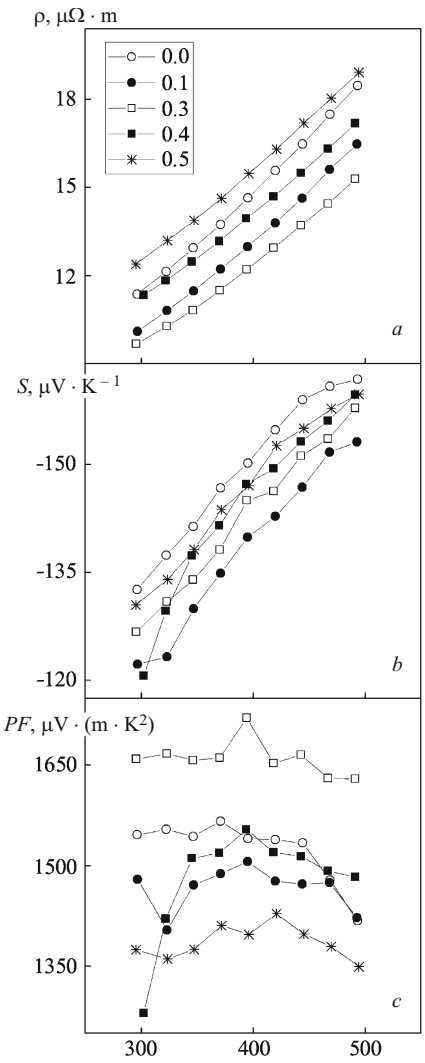

Fig. 6. Temperature dependences of electrical resistivity (*a*), Seebeck coefficient (*b*) and power factor (*c*) for the composites $Bi_2Te_{2.7}Se_{0.3}$ + Fe with different weight content of the filler: 0; 0.1; 0.3; 0.4 and 0.5% Fe.

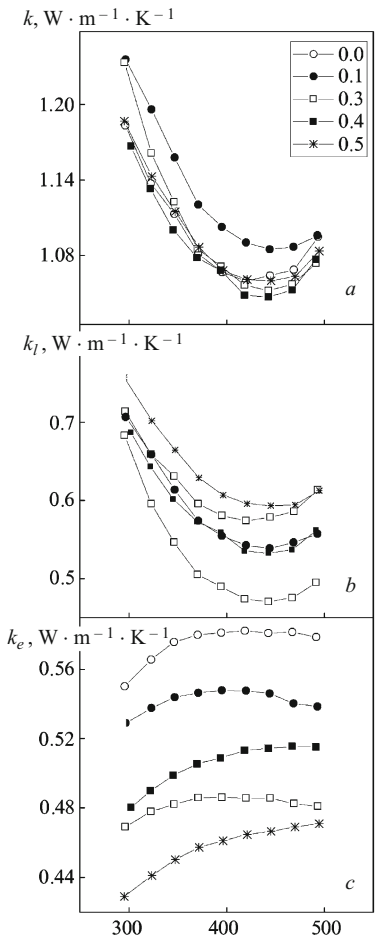

Fig. 7. Temperature dependences of the total thermal conductivity (*a*), lattice thermal conductivity (*b*), and electronic thermal conductivity (*c*) for samples of the composite $Bi_2Te_{2.7}Se_{0.3}$ + Fe with different weight content of the filler: 0; 0.1; 0.3; 0.4; and 0.5% Fe.

The temperature dependences of electrical resistivity (Fig. 6*a*), the Seebeck coefficient (Fig. 6*b*) and power factor $PF = S^2/\rho$ (Fig. 6*c*) of the composite $Bi_2Te_{2.7}Se_{0.3}$ + Fe samples with different content of the filler are shown in Fig. 6. These dependences are typical for compounds based on Bi_2Te_3 [14 – 16].

For samples of all compositions, an increase in temperature effects a gradual rise in electrical resistivity. Such a temperature evolution of resistance is observed for metals or degenerate semiconductors. In this case, the electron concentration does not depend on temperature, and the dependence $\rho(T)$ is determined by the temperature dependence of the electron mobility. For the investigated temperature range, as the temperature increases, the mobility decreases due to the scattering of electrons by acoustic and optical phonons, which effects gradual growth of electrical resistivity with increasing temperature. The electrical resistivity depends non-monotonically on the filler content. As the Fe concentration increases, the resistance first decreases and then increases, i.e. the minimum resistance value corresponds to a sample with 0.3 wt.% Fe.

The Seebeck coefficient for all composite samples is negative, which corresponds to electronic type conductivity. For all compositions, the Seebeck coefficient increases linearly with rising temperature and gradual saturation at maximum temperature. This behavior is typical for degenerate electronic semiconductors. The observed deviation from linear growth is associated with the onset of intrinsic conduction at high temperatures, during which electron-hole pairs begin to be thermally generated (the sign of the Seebeck coefficient for holes is positive). Of note, the Seebeck coefficient weakly depends on the filler content in the composite system $Bi_2Te_{2.7}Se_{0.3}$ + Fe system. The power factor takes into account the contributions from temperature changes in electrical resistivity and the Seebeck coefficient. Since the Seebeck coefficient weakly depends on the mass content of

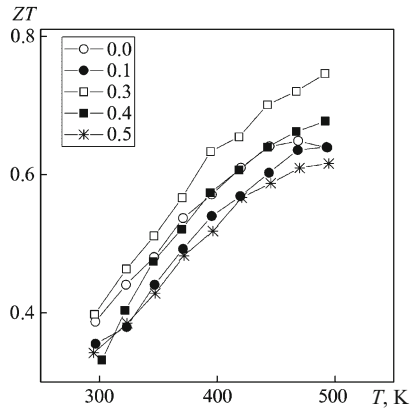

Fig. 8. Temperature dependences of thermoelectric figure of merit for specimens of $Bi_2Te_{2.7}Se_{0.3}$ + Fe composite with different weight content of filler: 0; 0.1; 0.3; 0.4 and 0.5% Fe.

the filler, and the electrical resistivity is minimal for the composite sample with 0.3% Fe, the maximum value of the power factor is achieved precisely for this sample (Fig. 6*c*).

Figure 7 shows the temperature dependences of the total thermal conductivity (Fig. 7*a*), lattice thermal conductivity (Fig. 7*b*), and electronic thermal conductivity (Fig. 7*c*) for samples of the composite $Bi_2Te_{2.7}Se_{0.3}$ + Fe with different weight content of filler (0; 0.1; 0.3; 0.4 and 0.5% Fe).

These dependences also have a form that is characteristic of compounds based on bismuth telluride. The dependences $k(T)$ for samples of all compositions show minima at about 430 K. The appearance of these minima is associated with a change in the heat conduction mechanism. The dependences $k_e(T)$ for electronic thermal conductivity determined using the Wiedemann–Franz law correlate with the dependences $\rho(T)$ shown in Fig. 6*a*. The lattice contribution to the total thermal conductivity was determined as $k_p(T) = k(T) - k_e(T)$. Like the total thermal conductivity, the lattice contribution has a minimum at about 430 K. For temperatures below the minimum, the lattice thermal conductivity decreases with increasing temperature. Above the Debye temperature the lattice thermal conductivity decreases with increasing temperature according to the law T^{-1}. In accordance with the Dulong–Petit law, in this case the lattice heat capacity does not depend on temperature. Then the phonon energy and the number of phonons increase linearly with increasing temperature. Since the scattering rate is proportional to the number of phonons, the lattice thermal conductivity will also decrease with increasing temperature. This mechanism determines the low-temperature behavior of the lattice thermal conductivity. It should be noted that the minimum value of lattice thermal conductivity is observed for a composite sample with 0.3 wt.% Fe. The growth of the lattice thermal conductivity above the minimum is due to the appearance and development of the contribution from the bipolar thermal conductivity.

The temperature dependences of ρ, S_2, and k were used to determine the temperature dependences of the thermoelectric figure of merit ZT of samples of the composite $Bi_2Te_{2.7}Se_{0.3}$ + xFe with different filler contents. The temperature dependences of the thermoelectric figure of merit for samples of all compositions behave in a similar way: as the temperature rises from room temperature, ZT increases with a gradual proneness to a constant value (Fig. 8). Such a proneness to saturation of the temperature dependence of ZT is associated with the onset of intrinsic conduction at high temperatures. The maximum values of the quality factor are observed at 500 K (the maximum temperature used in the measurements).

The composition with filler weight content 0.3% Fe has a higher figure of merit compared to $Bi_2Te_{2.7}Se_{0.3}$ matrix. For this composition, the maximum value of ZT reaches about 0.75, while for *ZT for* $Bi_2Te_{2.7}Se_{0.3}$ does not exceed about 0.63. So, in the composite system $Bi_2Te_{2.7}Se_{0.3}$ + Fe the thermoelectric figure of merit can be increased by about 20%.

CONCLUSIONS

Samples of the ceramic-metal composite $Bi_2Te_{2.7}Se_{0.3}$ + Fe with different weight content of the filler (0; 0.1; 0.3; 0.4 and 0.5% Fe), in which the filler forms inclusions of the core–shell type (Fe@$FeTe_2$), were obtained. The influence of the filler content on the features of the microstructure and thermoelectric properties of the composites was analyzed. A composite with weight content 0.3% Fe has a thermoelectric figure of merit 20% higher than for the material of the composite matrix. The detected change in the thermoelectric properties of the composite can be associated with the following factors:

1) change in the electron concentration, which is associated with a change in the internal structure of Fe@$FeTe_2$ inclusions;

2) electron and phonon scattering by inclusions;

3) electron scattering by the magnetic moments of ferromagnetic cores of inclusions.

This work was financially supported by the Russian Science Foundation, grant No. 21-12-00405, using the equipment of the Center for the Collective Use of Scientific Equipment "Technologies and Materials" of the National Research University "BelGU."

REFERENCES

1. O. Ivanov, M. Yaprintsev, A. Vasil'ev, et al., "Features of microstructure and thermoelectric properties of the cermet composites based on grained Bi_2Te_3 matrix with locally-gradient Ni@$NiTe_2$ inclusions," *Chin. J Phys*., **77**, 24 – 35 (2022).
2. M. Zhezhu, A. Vasil'ev, M. Yaprintsev, et al., "Effect of spark plasma sintering temperature on microstructure and thermoelectric properties of the cermet composites consisting of

$Bi_2Te_{2.1}Se_{0.9}$ matrix and Co@$CoTe_2$ inclusions," *J. Sol. State Chem*., **305**. 122696: 1 – 9 (2022).
3. O. N. Ivanov, M. N. Yapryntsev, A. E. Vasil'ev, et al., "Microstructure features of metal-matrix composites based on thermoelectric bismuth telluride matrix and ferromagnetic filler," *Glass Ceram*., **78**(11 – 12), 442 – 447 (2021).
4. H. J. Goldsmid, "Bismuth telluride and its alloys as materials for thermoelectric generation," *Mater.*, **7**, 2577 – 2592 (2014).
5. S. D. Bhame, D. Pravarthana, W. Prellier, and J. G. Noudem, "Enhanced thermoelectric performance in spark plasma textured bulk *n*-type $Bi_2Te_{2.7}Se_{0.3}$ and *p*-type $Bi_{0.5}Sb_{1.5}Te_3$," *Appl. Phys. Lett*., **102**, 2190:1 – 3 (2013).
6. X. A. Fan, J. Y. Yang, R. G. Chen, et al., "Characterization and thermoelectric properties of *p*-type 25% Bi_2Te_3 – 75% Sb_2Te_3 prepared via mechanical alloying and plasma activated sintering," *J. Phys. D. Appl. Phys.*, **39**, 740 – 745 (2006).
7. J. Jiang, L. Chen, S. Bai, et al., "Fabrication and thermoelectric performance of textured *n*-type $Bi_2(Te, Se)_3$ by spark plasma sintering," *Mater. Sci. Eng. B*, **117**, 334 – 338 (2005).
8. Q. Lognon, F. Gascoin, O. I. Lebedev, et al. "Quantitative texture analysis of spark plasma textured *n*-Bi_2Te_3," *J. Am. Ceram. Soc*., 2014. **97**, 2038 – 2045.
9. T. A. Fabijanic, S. Takovlijvic, M. Franz, and I. Jeren, "Influence of grain growth inhibitors and powder size on the properties of ultrafine and nanostructured cemented carbides sintered in hydrogen," *Metals*, **6**, 198 – 204 (2016).
10. L. Eglite, M. Antonova, E. Birks, et al., "Grain growth in $Na_{0.5}Bi_{0.5}TiO_3$-based solid solutions," *Integrated Ferroelectrics*, **196**, 112 – 119 (2019).
11. L. Wang, V. Pouchly, K. Maca, et al., "Intensive particle rearrangement in the early stage of spark plasma sintering process," *J. Asian Ceram. Soc*., **3**, 183 – 187 (2015).
12. I. Alvarez-Clemares, G. Mata-Osoro, A. Fernandez, et al., "Transparent alumina/ceria nanocomposites by spark plasma sintering," *Adv. Eng. Mater.*, **12**, 1154 – 1160 (2010).
13. Y. Liu, Y. Zhang, K. H. Lim, et al., "High thermoelectric performance in crystallographically textured *n*-type $Bi_2Te_{3-x}Se_x$ produced from asymmetric colloidal nanocrystals," *ACS Nano*., **12**, 7174 – 7184 (2018).
14. X. H. Ji, X. B. Zhao, and Y. H. Zhang, "Synthesis and properties of rare earth containing Bi_2Te_3 based thermoelectric alloys," *J. Alloys Compd*., **387**, 282 – 286 (2005).
15. F. Wu, H. Song, J. Jia, and X. Hu, "Effects of Ce, Y, and Sm doping on the thermoelectric properties of Bi_2Te_3 alloy," *Prog. Nat. Sci. Mater. Int*., **23**, 408 – 412 (2013).
16. F. Wu, H. Z. Song, and J. F. Jia, "Thermoelectric properties of Ce-doped *n*-type $Ce_xBi_{2-x}Te_{2.7}Se_{0.3}$ nanocomposites," *Phys. Stat. Sol. A*, **210**, 1183 – 1189 (2013).